International Journal of Mass Spectrometry 295 (2010) 138–144

Contents lists available at ScienceDirect

International Journal of Mass Spectrometry

journal homepage: www.elsevier.com/locate/ijms

Differential mobility spectrometry/mass spectrometry: The design of a new mass spectrometer for real-time chemical analysis in the field

Manuel J. Manard[a,*], Rusty Trainham[a], Stephan Weeks[a], Stephen L. Coy[b], Evgeny V. Krylov[b], Erkinjon G. Nazarov[b]

[a] National Security Technologies, LLC, Special Technologies Laboratory, 5520 Ekwill St., Santa Barbara, CA 93111, United States
[b] Sionex Corporation, 8-A Preston Court, Bedford, MA 01730, United States

ARTICLE INFO

Article history:
Received 27 January 2010
Received in revised form 25 March 2010
Accepted 29 March 2010
Available online 3 April 2010

Keywords:
Portable mass spectrometer
Differential mobility spectrometry
Miniature ion funnel

ABSTRACT

The design of a prototype, field-portable mass spectrometer (MS) is described. The MS has been designed with an atmospheric interface in order to couple the system to a commercially available differential mobility spectrometer. The differential mobility spectrometer provides selective injection of trace-level analytes of interest into the inlet of the MS for real-time chemical detection. To accomplish this task, the MS design incorporates the use of an electrodynamic ion funnel to transport the ion beam, generated at atmospheric pressure, to the high-vacuum chamber that houses the mass analyzer. This leads to a design that utilizes two stages of differential pumping to achieve an overall pressure drop from atmosphere (760 Torr) to approximately 1×10^{-5} Torr. A mass resolution of 140 ($m/z = 84$) and a limit of detection of approximately 1 ppb_v have been measured for the system.

1. Background

For the past 15 years, there has been a growing effort to bring mass spectrometers (MSs) into the field [1–9]. This can primarily be attributed the technique's ability to rapidly detect and identify virtually any chemical species of interest with high precision and accuracy. MSs have been deployed in environments that vary from under water [10–13] to outer space [14–16]. The increased portability of MS systems can be partially attributed to recent advances in vacuum pump and detection technologies. These advances have decreased the size, weight, power and vacuum requirements of these essential components, without significantly reducing the overall performance of the devices. As a result, the analogous physical parameters (size, weight, etc) of MSs have also been reduced, leading to significant miniaturization and increased fieldability [17,18].

Despite recent advances, MS miniaturization is not without its pitfalls. It has been observed that reducing the size of analytical instrumentation can have a negative impact on performance [19,20]. The sensitivity, mass resolution and mass range are a few parameters that suffer from MS miniaturization. Furthermore, for direct atmospheric sampling systems, mass spectra can become exceedingly complex when multiple chemical species are simultaneously introduced to the system. This leads to complicated data analysis and could result in the missed detection of a target analyte that is present at low concentration levels or lead to a false positive identification.

It has been previously shown that integrating multiple analytical techniques into a single instrument can compensate for the negative effects of instrumental miniaturization and provide complimentary information that can aid in chemical identification [21–23]. One technique with the potential to contribute complimentary information to mass spectral analysis is differential mobility spectrometry (DMS) [24,25]. DMS can operate as a continuous ion filter at ambient pressure and is currently used for the separation and detection of chemical reagents with a field-portable system [26–29]. Numerous research efforts have focused on interfacing DMS to mass spectrometry due to its ion-separation capabilities. Currently, there are several areas of research where DMS has been successfully interfaced to a MS and the benefits of coupling the two techniques have been discussed [30–36]. These interfaces have largely been to laboratory scale instruments. However, Sionex has also designed interfaces that have been used successfully for pulsed and low-flow instruments [37]. These applications of DMS to mass spectrometry have all found DMS effective in reducing chemical noise, separating isobaric ions and charge states, and improving the accuracy of quantitative measurements in complex samples.

Here, we present the design of a prototype, field-portable MS system with an atmospheric interface devised to couple directly to a DMS unit. For this system, DMS serves as a tunable chemical filter, separating target compounds from complicated mixtures

* Corresponding author. Tel.: +1 805 681 2121; fax: +1 805 964 3416.
E-mail address: manardmj@nv.doe.gov (M.J. Manard).

1387-3806/$ – see front matter © 2010 Elsevier B.V. All rights reserved.
doi:10.1016/j.ijms.2010.03.011

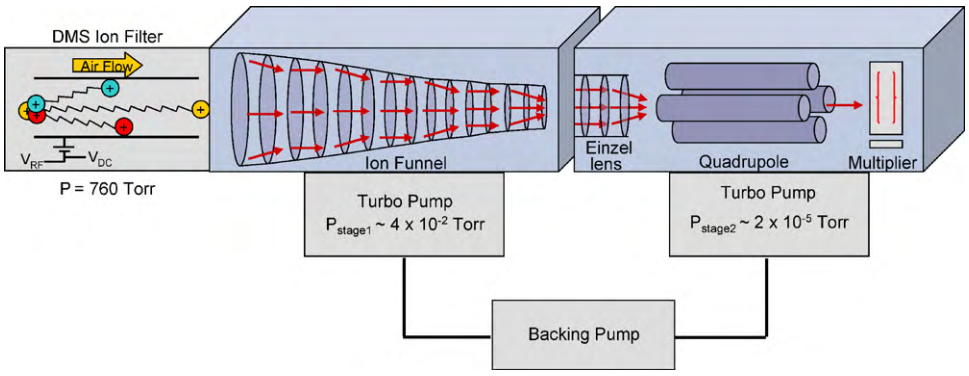

Fig. 1. A schematic diagram of the MS system design.

so that only analytes of interest are injected into the MS. This is accomplished by utilizing the nonlinear dependence of an ion's mobility coefficient on the RF electric field strength. The current MS instrumentation uses two-stage differential pumping to couple the atmospheric sampling/separation region with the high-vacuum, mass analysis portion of the instrument. The critical component of the system's design is the use of an electrodynamic ion funnel [38–40], which guides and focuses the ion beam through the first stage of differential pumping. The performance of the system in its current configuration is discussed below.

2. The instrument

2.1. DMS

A schematic representation of the MS system is shown in Fig. 1. Ions are generated at ambient pressure using a variety of ionization sources, but the radioactive ^{63}Ni source is most commonly used with DMS units to ionize incoming compounds. Once ions exit the ionization chamber, they are carried by a gas stream to the mobility-filtering region of the unit. The design details of the DMS system have been given previously [27,29,41], and only a brief description will be presented here. A typical flow rate through DMS units for field-portable applications is approximately 300 mL/min. The DMS filtration region is designed based on resolution and sensitivity constraints using a MATLAB software application that implements the performance characteristics of DMS. The filter for this instrument consists of two parallel DMS analytical plates, each measuring 10 mm × 1.5 mm, spaced 0.5 mm apart. Here, ions are subjected to an asymmetric, alternating RF electric field. Specifically, the ions experience a high field normal to the plates for a short time alternating with a low field in the opposite direction for a longer time. The time averaged field is zero. The mobility of an ion in a high electric field (>10,000 V/cm) is generally not independent of field and, more important, is different than the low field mobility. This results in some net velocity toward one of the plates which will remove the ion. Ions of a particular species will be transmitted if an additional DC compensation voltage (CV) is superimposed on the RF field to null out this velocity [24]. Ions of different species will be transmitted with different compensation voltages, allowing particular target analytes to be rapidly selected.

The ion mobility dependence on the electric field is given by Eq. (1) [42,43],

$$K\left(\frac{E}{N}\right) = K(0)\left(1+\alpha\left(\frac{E}{N}\right)\right) \cong K(0)\left(1+\sum_{k=1}^{N}\alpha_{2k}\left(\frac{E}{N}\right)^{2k}\right) \quad (1)$$

where $K(0)$ is the mobility of an analyte in the low field limit, E/N is the ratio between the electric field and the gas density, and α_{2k} are analyte-dependent coefficients. Ions that successfully traverse the filtration region are then focused into the MS. DMS ion filtration is sensitive to the normalized field dependence of mobility, $\alpha(E/N)$, in Eq. (1). The advantage of this technique over others that use a similar scheme, such as gas chromatography/mass spectrometry (GC/MS), is that separations using DMS occurs in 1–4 ms, while separations using modern, low thermal mass GC columns typically require times of at least 3–5 min. Additionally, sweeping the CV applied to the DMS unit allows different components to enter the mass spectrometer at different times, essentially generating individual, time-separated mass spectra for identifying multiple target analytes present in the sampled atmosphere (again, similar to GC/MS but requiring much less time).

2.2. Vacuum design

As previously mentioned, the MS was designed to have two stages of differential pumping to facilitate a pressure reduction from 760 Torr to the pressure regime required for proper operation of the mass analyzer and the detector (approximately 10^{-5} Torr). In order to generate the vacuum for the system, two Varian turbo pumps (Turbo-V 81 M) with pumping speeds equal to 50 L/s, backed by a single Varian rotary vane rough pump (DS-42), were mounted to two 2-3/4 in. Conflat flange five-way crosses. These vacuum chambers house the ion focusing and mass analysis components of the instrument. The vacuum chambers are joined together by a modified double-side 2-3/4 in. Conflat flange.

Two conductance-limiting orifices were used to allow ions to move between sections of the instrument, while simultaneously limiting the flow of background gas into the two vacuum chambers. The pinholes are generated using stainless steel foils measuring 0.001 in. thick (Edmund Optical). To provide structural support, the foils are mounted onto stainless steel discs using a conductive epoxy. The foils are placed in a grove that is machined into the support discs. Additionally, the support discs have 1 mm clearance holes drilled on center. The first orifice measures 0.1 mm in diameter and is mounted to the inlet flange of the MS. The second orifice is mounted to the double-sided Conflat flange that joins the vacuum chambers. Initially, a 0.2 mm diameter pinhole was used at this junction. However, the size of this pinhole has subsequently been increased to 0.4 mm for improved ion transmission into the second vacuum chamber. In both cases, a compressed O-ring is used to generate a seal between the pinhole assemblies and the vacuum hardware.

The measured pressure of the first vacuum chamber is approximately 4×10^{-2} Torr when opened to ambient pressure. Similarly, a 0.2 mm orifice generates an operating pressure in the second vacuum chamber of approximately 6×10^{-6} Torr. When replaced with

Fig. 2. Ion focusing assembly. The ion funnel spacers and the printed circuit board are shown on the left and the Einzel lenses and ceramic spacers are shown on the right. Both ion focusing elements are mounted to a modified, double-sided 2-3/4 in. Conflat flange.

the 0.4 mm orifice, the pressure of this region rises to just above 10^{-5} Torr.

2.3. Ion optics

Ion trajectories were simulated using Simion 8 [44], to predict the optimal configuration of ion guiding/focusing electrodes for maximized ion transmission through the system. The resulting, custom-built ion optics assembly is shown in Fig. 2. In the high-vacuum chamber, three sets of Einzel lenses, having 4 mm inner diameters and placed 4 mm apart, are used to focus the beam into the mass analyzer of the system.

Ion focusing in the first vacuum chamber, where the mean-free-path of the beam (approximately 1 mm at 4×10^{-2} Torr) is less than the distance being traversed (approximately 13 cm), is accomplished using an ion funnel. The ion funnel functions by applying a DC ramp potential to a series of resistively coupled ring electrodes. An RF field is superimposed over the DC potential, with every other lens in the stack receiving the RF field. The lenses not connected to the RF portion of the circuit are held at the DC ramp potential. The DC ramp serves to guide the ion beam toward the entrance to the second vacuum chamber, while the RF electric field serves to axially re-center the ion beam when collisions with background gas molecules occur.

The configuration described above is not typical for applying RF to an ion funnel. Generally, RF is applied to all lenses in the stack. A transformer is generally used so that the RF applied to each electrode is 180° out of phase with its nearest neighbor. Our configuration was chosen to simplify the RF delivery circuitry. However, Simion simulations show that ion transmission through the funnel is unaffected as long as the amplitude of the RF is increased by approximately a factor of two.

For our system, 48 lenses make up the ion funnel assembly. The lenses in the stack are each 1 mm thick and are separated by 1.5 mm. The first five lenses, located at the entrance to the funnel, have inner diameters of 10 mm. This diameter is reduced to 9.5 mm for the next five lenses in the series. Following the first 10 lenses of the funnel, the inner diameters of each set of four lenses in the stack are reduced by 0.5 mm, until a diameter of 5 mm is reached. The final two lenses in the stack have inner diameters of 4 and 3 mm respectively. They are held at the same DC potential and are not coupled to the RF field. Similar configurations have been reported in the literature [39]. Here, it is used to aid in focusing the beam through the exit orifice. All lenses are held in place and electrically isolated from one another using custom-built, Delrin spacers. Both the DC and RF fields are applied to the lenses by a printed circuit board mounted directly to the spacers. The board uses 5 kΩ resistors in series to supply the DC field and 0.01 μF capacitors in parallel to supply the RF voltage. A series of spring-loaded pins push against each lens in the stack to generate the electrical contact. Typically, a frequency of approximately 1 MHz is applied to the ion funnel with an amplitude of 30 V_p. This RF amplitude is not sufficient to maximize ion transmission through the funnel at the operating pressure of 4×10^{-2} Torr. A redesign of the circuit board is currently being performed to increase the maximum RF amplitude that can be applied to the funnel. The DC potential is generally set to 50 V at the entrance to the funnel and 20 V at its exit. All DC voltages are delivered to the system using Agilent E3647A power supplies. The RF is supplied to the funnel using an Agilent function generator (Model 33250A) and a Tegam power amplifier (Model 2340).

2.4. Mass analysis

Mass analysis and detection are accomplished using a modified, commercially available Stanford Research Systems RGA200 quadrupole mass analyzer and a Channeltron electron multiplier detector. The quadrupole used in this system has a mass range of 1–200 amu. In order to focus the beam into the quadrupole, holes were cut into the repeller and anode grid assemblies in the commercial unit. The quadrupole can still be used as an RGA for diagnostic purposes by energizing the ionizer region of the probe. When an ion beam generated by external ionization sources is introduced to the quadrupole via the upstream components of the system, the ionizer region is not activated.

3. Results

3.1. Electron impact mass spectra

Initially, the ion funnel was tested independently from the rest of the system to determine the efficiency of its unconventional design. To facilitate these experiments, a Burle 4869 Channeltron electron multiplier was placed in the second vacuum chamber. Any ions transmitted into the second vacuum chamber by the ion funnel would be detected by the Channeltron. Additionally, for these preliminary studies, ions were generated using an electron impact source placed near the entrance of the ion funnel. The kinetic energy of the electron beam was set to approximately 36 eV. A variable leak valve was used to pressurize the vacuum chamber that houses the ion source and funnel to between 10^{-4} and 10^{-2} Torr with either argon or krypton. This experimental arrangement allowed us to study the effects of pressure on ion transmission through the funnel.

Ion currents of up to 5 μA were measured by the Channeltron detector. Correcting for the gain of the Channeltron, this corresponds to approximately 10^7 ions/s impacting the detector. From this value, a transmission efficiency of approximately 10–20% was calculated for the ion funnel. This is in good agreement with what was predicted by the ion trajectory simulations. The ion funnel is crucial to ion transmission through the first vacuum chamber. By simply removing the RF from the funnel, ion transmission is observed to decrease to nearly zero at the operating pressure of 10^{-2} Torr. Additionally, to maintain efficient ion transport through the funnel in the 10^{-4}–10^{-2} Torr pressure regime, the amplitude of the RF field must increase as the pressure increases. Once the optimal value of the RF frequency was determined, it was not observed to be affected by varying the pressure in this range.

Following the successful testing of the ion funnel, the complete MS system was assembled to obtain mass spectra for a variety of

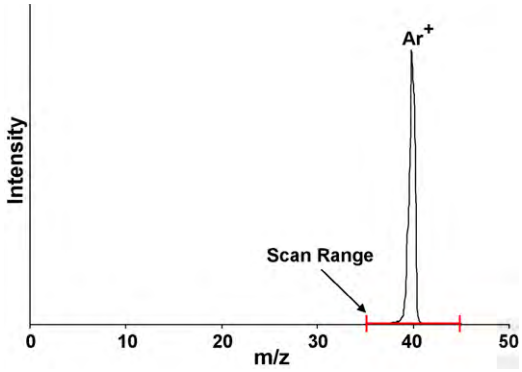

Fig. 3. Mass spectrum of Ar^+ acquired with an electron impact source. The scanned mass range is shown as the highlighted region.

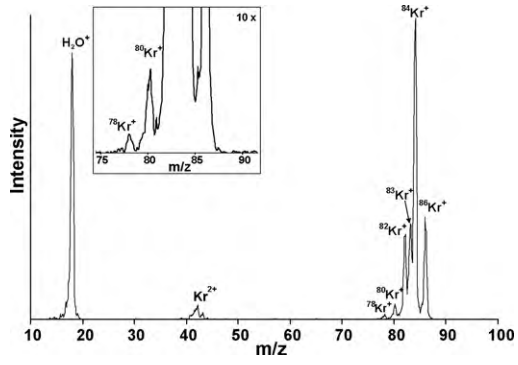

Fig. 4. Mass spectrum of Kr^+, Kr^{2+}, and H_2O^+ acquired with an electron impact source. The insert shows a blow up of the $^{78}Kr^+$ and $^{80}Kr^+$ isotopic species, which make up only 2.6% of naturally occurring Kr.

test chemicals. Accordingly, mass spectra for argon and krypton are shown in Figs. 3 and 4, respectively. The mass spectrum of Ar^+ (Fig. 3) was one of the first produced by the instrument. An excellent signal-to-noise ratio for the peak at $m/z = 40$ is observed. For this measurement, the quadrupole was scanned over a narrow m/z range ($m/z = 35$–45).

In order to experimentally determine the mass resolution of the instrument, a noble gas with multiple naturally occurring isotopes was used. Fig. 4 shows the mass spectrum of Kr^+. Note that Kr^{2+} and H_2O^+ are also observed in this mass spectrum. The distribution for naturally occurring isotopes of Kr is: ^{78}Kr (0.35%), ^{80}Kr (2.25%), ^{82}Kr (11.6%), ^{83}Kr (11.5%), ^{84}Kr (57.0%), and ^{86}Kr (17.3%). It is apparent from Fig. 4 that all Kr isotopes are observed and are present in approximately the proper distribution. The magnified insert clearly shows that even the $^{78}Kr^+$ ion, representing only 0.35% of naturally occurring Kr, is easily detected and resolved by the MS system. Furthermore, the mass resolution of the system can be determined from the mass spectrum. From Fig. 4, one can see that the peak at $m/z = 83$ is easily resolved from $m/z = 84$, which is approximately 5 times more abundant. From the separation between these two peaks, we calculate a mass resolution of 0.5 amu at 20% of the peak height. Or, for $m/z = 84$, this corresponds to a resolving power of 140 at FWHM. This is a reasonable result for a portable MS system.

3.2. Atmospheric sampling mass spectra

An atmospheric sampling ionization source was used to probe the performance of the system. Initially, a simple discharge source was utilized to produce ions at the inlet of the MS. The flow produced as a result of the pressure differential (approximately 90 mL/min, orifice diameter = 0.1 mm) carries ions into the first vacuum chamber. The mass spectrum produced from this study is shown in Fig. 5. To aid in ion formation, the sampled atmosphere was doped with a small amount of acetone that was placed on the tip of a cotton swab. The swab was situated near the inlet orifice of the system. The data clearly shows that an abundance of H_2O^+ ($m/z = 18$) is formed from this process. $H_2O^+(N_2)$, $H_2O^+(N_2)_2$ ($m/z = 46$ and 74, respectively) and H_2O^+(acetone) ($m/z = 76$) adduct ions are also observed. Additionally, a small amount of H_3O^+ is observed at the base of the H_2O^+ peak.

Table 1
Gas-phase chemistry leading to the formation of positively charged reactant ions in air by ^{63}Ni.

$N_2 + e^- (67\,keV) \rightarrow N_2^+ + 2e^-$
$N_2^+ + 2N_2 \rightarrow N_4^+ + N_2$
$N_4^+ + H_2O \rightarrow 2N_2 + H_2O^+$
$H_2O^+ + H_2O \rightarrow H_3O^+ + OH$
$H_3O^+ + H_2O + N_2 \rightarrow H^+(H_2O)_2 + N_2$
$H^+(H_2O)_2 + H_2O + N_2 \rightarrow H^+(H_2O)_3 + N_2$
$H^+(H_2O)_{n-1} + H_2O + N_2 \rightarrow H^+(H_2O)_n + N_2$

For details, see Ref. [45].

3.3. ^{63}Ni source atmospheric sampling mass spectra

The following set of experiments related to atmospheric sampling mass spectrometry was carried out using a ^{63}Ni ionization source in a stream of dry nitrogen. There are three reasons to use this radioactive beta emitter as a source in the current project: (1) well-known ion chemistry, (2) similarity to existing mobility-based devices, and (3) in-field calibration. Each of these points is discussed below.

3.3.1. Well-known ion chemistry

Ions formed by a ^{63}Ni source result from a series of well-known ion-neutral reactions and yield predictable mass spectra for small molecules. For example, Table 1 shows the gas-phase processes leading to the formation of positively charged reactant ion species inside the ^{63}Ni source. Proton affinities of the participating species control the proton transfer reactions to trace analytes. Thus, the theoretical yield of analyte ions produced by the gas-phase ion-molecule reactions can be estimated, allowing the mass spectra from the ^{63}Ni source to be predicted. The comparison between the theoretical and experimental mass spectra could provide valuable insight for estimating the analytical performance of system.

3.3.2. Similarity to existing mobility-based devices

This prototype MS is intended to be used for the detection and identification of chemical warfare agents (CWA), volatile explosives and toxic industrial components (TICs and TIMs) in the field. Ion mobility spectrometers (IMS) have been used in the field for these applications since 1980 and generally use ^{63}Ni sources. This source is ideal for ionization of trace vapors under these potentially harsh conditions. It requires no power, has low source noise, negligible weight and physical size, long life, and provides stable ion formation. A great deal of experimental data and design experience is available that can be adapted to a portable MS equipped with this source.

3.3.3. Calibration under in field conditions

Atmospheric pressure ionization (API) sources can be easy interchanged. This enables the use of different types of API sources, including corona, radioactive, ESI, DESI, DART, and surface sampling probes (SSP) among others. The choice of API source is determined by the needs of the application. In harsh environments, multisource measurements can be useful. The ^{63}Ni source is useful both as a primary source and as a secondary source, providing mass and sen-

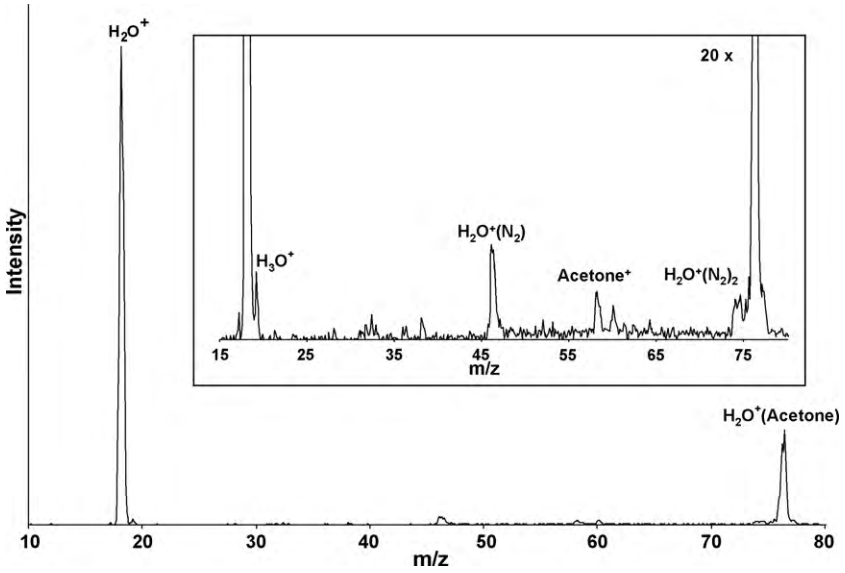

Fig. 5. Mass spectrum of H_2O^+, H_3O^+, acetone$^+$ and H_2O^+ clustering to both N_2 and acetone, respectively, acquired at atmospheric pressure using a discharge source. The insert shows a blow up of the low concentration ionic species. Acetone was used as a dopant to generate the mass spectrum shown.

sitivity calibration as well as verification of the overall health of the system.

Fig. 6 shows mass spectra obtained using a ^{63}Ni source without DMS pre-filtering. Spectrum 1 was obtained by passing dry nitrogen through the source. This background mass spectrum contains the expected protonated water clusters $H^+(H_2O)_n$ (n = 1–3) at m/z = 19, 37, and 55, respectively. This data is consistent with the ion chemistry shown in Table 1. The relative intensity of these peaks and the number of cluster species depend on the moisture level. Under our conditions (approximately 10 ppm_v of moisture) only the n = 1–3 cluster peaks are observed, with the major peak being the proton bound dimer $H^+(H_2O)_2$. Adding trace concentrations of chemicals to the air stream, such as acetone at sub-ppm_v levels, dramatically alters the mass spectrum. In spectrum 2, peaks related to water cluster ions have almost disappeared and peaks related to protonated acetone species, with m/z = 59 for H^+(acetone) and m/z = 117 for $H^+(acetone)_2$, are observed. The relative peak intensity between the protonated monomer and proton bound dimer depends on concentration. Peaks with m/z = 73, 87 and 101 are tentatively identified as $H^+(acetone(CH_2)_m)$ (m = 1–3) adduct ions and are detected only at relatively high acetone concentrations. At low ppb_v levels, the mass spectra contain both the protonated water clusters and analyte related peaks, as expected from the proton transfer mechanism.

A small amount of toluene, approximately 100 ppb_v, was introduced into the sample gas stream. The resulting data is shown in spectrum 3 of Fig. 6. The protonated toluene peak (m/z = 93) is observed in the mass spectrum as well as a small amount of protonated ethylbenzene impurity (m/z = 107). From the relative intensity of the toluene and ethylbenzene peaks, the impurity peak is estimated to be present at about 10% of the concentration of toluene. This data suggests that the MS system, when combined with a ^{63}Ni source, has an acceptable level of sensitivity for the detection of relatively low concentration analytes. Although the true concentration of ethylbenzene is unknown, the detection of a species with an implied concentration of approximately 10 ppb_v suggests that the MS design is suitable for the detection of trace-level target analytes.

Spectrum 4 of Fig. 6 shows the data for a mixture of low concentration, organic species. The mixture is comprised of acetone, benzene and acetonitrile. The data illustrates that when the total concentration of organic molecules is less than 0.1 ppm_v, multiple analyte ion species can be simultaneously observed in the mass spectrum. Accordingly, spectrum 4 contains all of the $H^+(H_2O)_n$ cluster ions (m/z = 19, 37 and 55 for n = 1–3, respectively), protonated acetonitrile (m/z = 43), the protonated acetone monomer (m/z = 59), and a double peak for benzene (m/z = 77 and 78, respectively). All ion species are easily detected and identified from the mass spectrum.

In order to determine the limit of detection of the MS, trace levels of dimethyl methylphosphonate (DMMP) were introduced to the MS system. A controlled measurement was made for the concentration of DMMP using a permeation tube source. The concentration of DMMP in the sample gas stream was approximately 1 ppb_v. Fig. 7 shows a mass spectrum of protonated DMMP (m/z = 125) acquired with the prototype MS and the ^{63}Ni source. Again, the characteristic $H^+(H_2O)_n$ peaks are observed in the spectrum. A signal-to-noise ratio for the peak in the mass spectrum is approximately 3:1, which is in accordance with standard analytical practices for the determination of the limit of detection for an instrument. This measured sensitivity is excellent for a field-portable MS system and is consistent with limits of detection reported for commercially available, portable GC/MS systems (Inficon). Additionally, this result provides evidence that, when the modifications are completed to the overall design of the MS, the instrument will have a limit of detection in the ppt_v level.

3.4. DMS/MS

A DMS unit was interfaced to the inlet of the prototype MS and the preliminary results are shown in Fig. 8. Again, a ^{63}Ni source is used to generate ions in a stream of nitrogen gas and a trace amount of acetone was added to the stream. Spectrum 1 of Fig. 8 shows data obtained in transport mode, where both the CV and the RF amplitude (V_{RF}) are set to zero. This is essentially the same as not having the DMS unit interfaced to the MS. The spectrum contains the protonated water monomer and dimer clusters at m/z = 19 and 37, respectively. Additionally, the protonated acetone peak at m/z = 59 is observed as the dominate feature of the mass spectrum and the peaks present at m/z = 73, 87 and 101 are tentatively identified as $H^+(acetone(CH_2)_m)$ (m = 1–3) adduct ions. This mass spectrum closely resembles the results shown in Fig. 6, spectrum 2 and is consistent with what would be expected for allowing all of these ionic species into the MS.

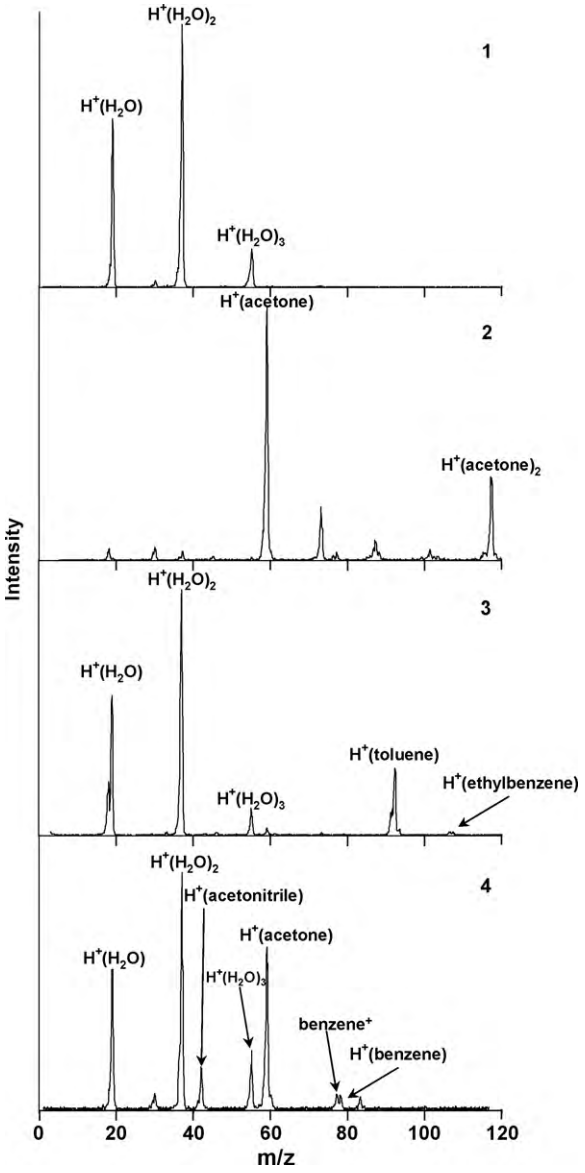

Fig. 6. API mass spectra for trace concentrations of chemicals in clean air; 1 – air (no chemicals), 2 – acetone in air, 3 – toluene in air, 4 – mixture of acetonitrile, acetone and benzene in air.

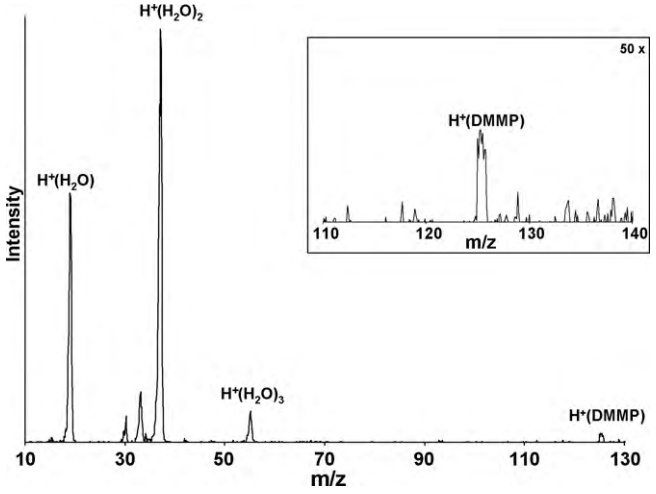

Fig. 7. Mass spectrum of $H^+(H_2O)_n$ (n = 1–3) and protonated DMMP acquired with a ^{63}Ni source at atmospheric pressure. The insert magnifies the DMMP peak, which has a measured concentration level of 1 ppb_v.

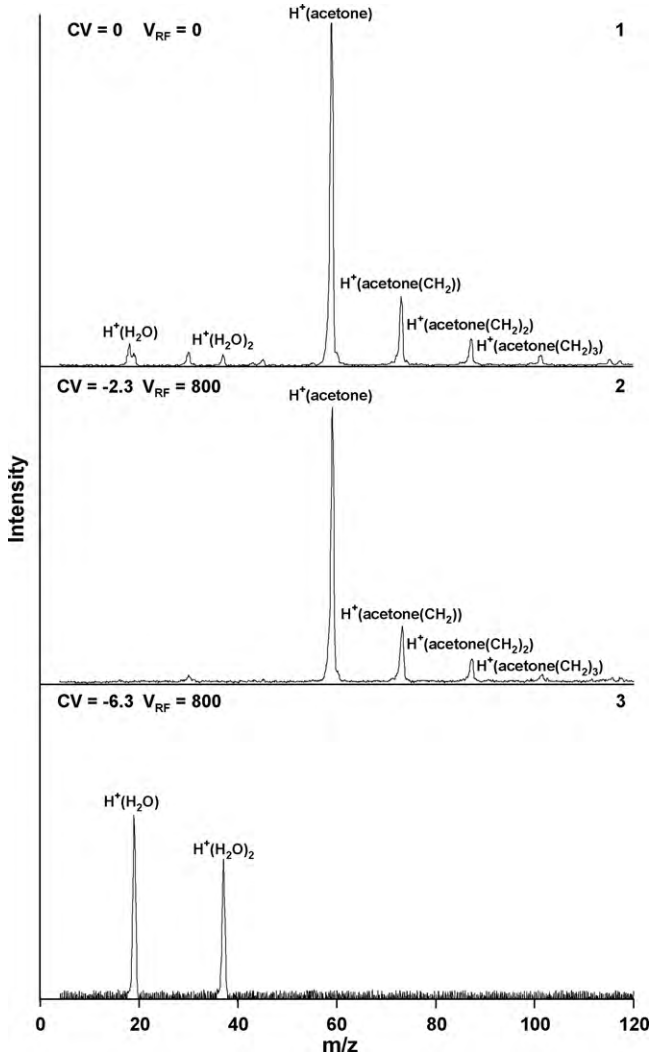

Fig. 8. DMS pre-filtered mass spectra for trace concentrations of acetone in clean air; 1 – CV = 0 and V_{RF} = 0 (no pre-filtering), 2 – CV = −2.3 and V_{RF} = 800, 3 – CV = −6.3 and V_{RF} = 800. All values reported for CV and V_{RF} are in units of volts.

In spectrum 2 of Fig. 8, a CV = −2.3 V and V_{RF} = 800 V was applied to the DMS unit. It is immediately clear that a very different mass spectrum is obtained. The peak intensities associated with the acetone ions are largely unchanged from the previous spectrum. However, the peaks associated with the protonated water clusters are completely removed from the mass spectrum. Furthermore, the CV and V_{RF} voltages applied to the DMS unit are consistent with what is observed for an acetone peak in a typical DMS spectrum. The data shown here strongly suggests that the DMS unit is effectively serving as an ion filter for the MS.

Following the acquisition of the data shown in Fig. 8, spectrum 2, a CV = −6.3 V was applied to the DMS unit while V_{RF} remained set to 800 V. These parameters correspond to the location of the protonated water clusters in a typical DMS spectrum. Spectrum 3 of Fig. 8 shows the resulting mass spectrum. Here, the protonated water clusters are present in the mass spectrum and the peaks associated with the acetone clusters have been removed. It is interesting to note that, although the protonated acetone monomer (m/z = 59) was the dominate feature of Fig. 8, spectrum 1, no trace of the peak

can be observed in spectrum 3 of Fig. 8. These results clearly indicate that the DMS unit serves as a highly efficient ion filter for the MS and that the combination of the two techniques could lead to a powerful device for the real-time separation and detection of target analytes.

4. Summary

A prototype, portable MS for real-time chemical detection of trace, gas-phase analytes has been designed and successfully bench tested. The system dimensions are currently $25'' \times 6'' \times 16''$ and its total weight is approximately 70 lb. The unit uses two stages of differential pumping to achieve an overall pressure drop from atmosphere to approximately 2×10^{-5} Torr. The MS system uses an electrodynamic ion funnel to focus and guide the ion beam through the first stage of differential pumping. Electrostatic Einzel lenses focus the beam in the second stage of differential pumping into the entrance of a commercial quadrupole mass filter, where the ions are mass selected and detected by a Channeltron electron multiplier. The DMS portion of the system was interfaced to the MS and highly efficient, selective ion injection into the MS has been demonstrated. The system has a mass resolution of 140 at FWHM ($m/z = 84$) and a limit of detection of approximately 1 ppb_v. Additional design modifications, such as redesigning the ion funnel circuit board so that higher RF amplitudes can be applied to the device to increase ion transmission, and improving the mass resolution of the system by decreasing the kinetic energy of the ion beam prior to introduction to the quadrupole, are currently being explored. These preliminary results are extremely promising and suggest that the fully realized DMS/MS system could likely provide laboratory quality data in the field and become a powerful instrument for the real-time detection of chemical species.

Acknowledgements

The author would like to acknowledge T. Keenan, J. Buckley, G. Anthony and M. Celmins for engineering contributions to the system as well as P.R. Kemper for helpful discussions regarding the design of the instrument.

This manuscript has been authored by National Security Technologies, LLC, under Contract No. DE-AC52-06NA25946 with the U.S. Department of Energy. The United States Government retains and the publisher, by accepting the article for publication, acknowledges that the United States Government retains a non-exclusive, paid-up, irrevocable, worldwide license to publish or reproduce the published form of this manuscript, or allow others to do so, for United States Government purposes. This work was also supported by the Columbia University Center for Medical Countermeasures against Radiation (Principal Investigator Prof. David Brenner), Project 3 (PI's Prof. A.J. Fornace, Jr. and J.R. Idle), and funded by NIH/NIAID grant U19 AI067773-04.

References

[1] V.T. Kogan, A.K. Pavlov, Y.V. Chichagov, Y.B. Tubol'tsev, G.Y. Gladkov, A.D. Kazanshii, V.A. Nikolaev, R. Pavlichkova, Field Anal. Chem. Technol. 1 (1997) 331.
[2] A.J. White, M.G. Blamire, C.A. Corlett, B.W. Griffiths, D.M. Martin, S.B. Spencer, S.J. Mullock, Rev. Sci. Instrum. 69 (1998) 565.
[3] M.P. Mcloughlin, W.R. Allmon, C.W. Anderson, M.A. Carlson, D.J. DeCicco, N.H. Evancich, Johns Hopkins APL Tech. Dig. 20 (1999) 326.
[4] C.C. Mulligan, N. Talaty, R.G. Cooks, Chem. Commun. 16 (2006) 1709.
[5] C.C. Mulligan, D.R. Justes, R.J. Noll, N.L. Sanders, B.C. Laughlin, R.G. Cooks, Analyst 131 (2006) 556.
[6] R.G. Cooks, Z. Ouyang, Z. Takats, J.M. Wiseman, Science 311 (2006) 1566.
[7] L. Gao, Q. Song, G.E. Patterson, R.G. Cooks, Z. Ouyang, Anal. Chem. 78 (2006) 5994.
[8] V.T. Kogan, A.K. Pavlov, Y.V. Chichagov, Y.V. Tubol'tsev, M.I. Savchenko, O.B. Smirnov, O.S. Viktorova, I.V. Viktorov, S.A. Vlasov, B.M. Dubenski, V. Nedvigin, Y. Gao, Exp Instrum. Tech. 77 (2007) 73.
[9] A. Keil, J. Hernandex-Soto, R.J. Noll, M. Rico, L. Gao, Z. Ouyang, R.G. Cooks, Anal. Chem. 80 (2008) 734.
[10] G.P.G. Kibelka, R.T. Short, S.K. Toler, J.E. Edkins, R.H. Bryne, Talanta 64 (2004) 961.
[11] R.T. Short, S.K. Toler, G.P.G. Kibelka, D.T. Rueda Roa, R.J. Bell, R.H. Byrme, Trends Anal. Chem. 25 (2006) 637.
[12] H.F. Hemond, A.V. Mueller, M. Hemond, J. Am. Soc. Mass Spectrom. 19 (2008) 1403.
[13] H. Hermond, J. Cheung, A. Mueller, J. Wong, M. Hermond, D. Mueller, J. Eskesen, Limnol. Oceanogr. Methods 6 (2008) 288.
[14] D. Meunier, R. Sternberg, F. Mettetal, A. Buch, D. Coscia, C. Szopa, C. Rodier, P. Coll, M. Cabanec, R. Raulin, Adv. Space Res. 39 (2007) 337.
[15] T. Evans-Nguyen, L. Becker, V. Doroshenko, R.J. Cotter, Int. J. Mass Spectrom. 278 (2008) 170.
[16] J.H. Hoffman, R.C. Chaney, H. Hammack, J. Am. Soc. Mass Spectrom. 19 (2008) 1377.
[17] L. Gao, R.G. Cooks, Z. Ouyang, Anal. Chem. 80 (2008) 4026.
[18] L. Gao, A. Sugiarto, J.D. Harper, R.G. Cooks, Z. Ouyang, Anal. Chem. 80 (2008) 7198.
[19] J. Xu, W.B. Whitten, J.M. Ramsey, Anal. Chem. 72 (2000) 5787.
[20] A.V. Mariano, W.S. Su, S.K. Guharay, Anal. Chem. 81 (2009) 3385.
[21] A.B. Kanu, H.H. Hill, J. Chromatogr. A 1177 (2008) 12.
[22] W. Cheung, Y. Xu, C.L.P. Thomas, R. Goodacre, Analyst 134 (2009) 557.
[23] A.B. Kaun, P. Dwivedi, M. Tam, L. Matz, H.H. Hill, J. Mass Spectrom. 43 (2008) 1.
[24] I.A. Buryakov, E.V. Krylov, E.G. Nazarov, U.K. Rasulev, Int. J. Mass Spectrom. Ion Process. 128 (1993) 143.
[25] S. Kendler, G.R. Lambertus, B.D. Dunietz, S.L. Coy, E.G. Nazarov, R.A. Miller, R.D. Stacks, Int. J. Mass Spectrom. 263 (2007) 137.
[26] H. Borsdorf, E.G. Nazarov, R.A. Miller, Anal. Chim. Acta 575 (2006) 76.
[27] R.A. Miller, G.A. Eiceman, E.G. Nazarov, A.T. King, Sens. Actuators B 67 (2000) 300.
[28] G.A. Eiceman, E.G. Nazarov, R.A. Miller, Int. J. Ion Mobil. Spectrom. 3 (2000) 15.
[29] B.B. Schneider, T.R. Covey, S.L. Coy, E.V. Krylov, E.G. Nazarov, Int. J. Mass Spectrom. (2010), doi:10.1016/j.ijms.2010.01.006.
[30] D.A. Barnett, B. Ells, R. Guevremont, R.W. Purves, J. Am. Soc. Mass Spectrom. 13 (2002) 1282.
[31] A.J.H. Borysik, P. Read, D.R. Little, R.H. Bateman, S.E. Radford, A.E. Ashcroft, Rapid Commun. Mass Spectrom. 18 (2004) 2229.
[32] M. McCooeye, L. Ding, G.J. Gardner, C.A. Fraser, J. Lam, R.E. Sturgeon, Z. Mester, Anal. Chem. 75 (2003) 2538.
[33] R.W. Purves, R. Guevremont, S. Day, C.W. Pipich, M.S. Matyjaszczuk, Rev. Sci. Instrum. 69 (1998) 4094.
[34] B.M. Kolakowski, Z.N. Mester, Analyst 132 (2007) 842.
[35] A.A. Shvartsburg, F. Li, K. Tang, R.D. Smith, Anal. Chem. 78 (2006) 3706.
[36] A.A. Shvartsburg, Differential Ion Mobility: Non-linear Ion Transport and Fundamentals of FAIMS, CRC Group/Taylor & Francis LLC, Boca Raton, FL, 2008.
[37] R.G. Cooks, Z. Ouyang, F.K. Tadjimukhamedov, Abstract 1470-1 Pittcon 2010, Orlando, FL, 2010.
[38] S.A. Shaffer, K. Tang, G.A. Anderson, D.C. Prior, H.R. Udseth, R.D. Smith, Rapid Commun. Mass Spectrom. 11 (1997) 1813.
[39] T. Wyttenbach, P.R. Kemper, M.T. Bowers, Int. J. Mass Spectrom. 212 (2001) 13.
[40] S.L. Koeniger, S.I. Merenbloom, S.J. Valentine, M.F. Jarrold, H.R. Udseth, R.D. Smith, D.E. Clemmer, Anal. Chem. 78 (2006) 4161.
[41] E.V. Krylov, E.G. Nazarov, R.A. Miller, Int. J. Mass Spectrom. 266 (2007) 76.
[42] E.A. Mason, E.W. McDaniel, Transport Properties of Ions in Gases, Wiley, New York, 1988.
[43] G.A. Eiceman, Z. Karpas, Ion Mobility Spectrometry, second ed., CRC Press/Taylor & Francis LLC, Boca Raton, FL, 2005.
[44] D.A. Dahl, Int. J. Mass Spectrom. 200 (2000) 3.
[45] A. Good, D.A. Durden, P. Kebarle, J. Chem. Phys. 52 (1970) 212.